Int. J. Heat Mass Transfer. Vol. 35, No. 9, pp. 2161–2172, 1992
Printed in Great Britain

0017–9310/92 $5.00 + 0.00

Modified enthalpy method applied to rapid melting and solidification

ALI A. ROSTAMI,† RALPH GREIF and RICHARD E. RUSSO

Mechanical Engineering Department and Applied Science Division, Lawrence Berkeley Laboratory, University of California at Berkeley, CA 94720, U.S.A.

(*Received* 12 *February* 1991 *and in final form* 30 *August* 1991)

Abstract—The rapid melting and solidification of a target material was studied. The enthalpy technique was used in an explicit finite difference form to calculate the location of the solid–liquid interface and the temperature distribution in the target. The technique was modified so that it is not necessary that the temperature of the mesh containing the interface remain constant at the melting point. Instead, by using the energy boundary condition at the interface a new value of the temperature of the grid point is calculated at every time step. The materials between two grid points that are on each side of the interface consist of two phases with considerably different thermal conductivities. The thermal resistances of the material between these grid points were calculated by treating the region as a composite material. The effects of the duration, the temporal shape and the intensity of the laser pulse on the rate of propagation of the phase change and on the temperature distribution were studied. The results of the numerical prediction for the melt depth created in an aluminum target with a 100 ns electron beam were compared with experimental data and good agreement was obtained.

INTRODUCTION

THE DETERMINATION of the heat transfer during a solid–liquid change of phase is of importance in problems relative to welding, coating, crystal growth, environmental engineering and chemical analysis. In many cases multidimensional variations are important, boundary conditions are complex, thermophysical properties vary with temperature and phase, volumetric heat sources may be present, and several mechanisms of heat transfer may take place. Thus analytical solutions [1–4] which exist for specific problems have a limited range of applicability. In order to solve these problems numerical methods are usually required.

A large number of numerical techniques have been developed to solve solid–liquid phase change problems. Extensive reviews of many analytical and numerical techniques can be found in Ockendon and Hodgkins [3], Shamsundar [5] and Salcudean and Abdullah [6]. The numerical methods used may be conveniently divided into two groups. In the first group the temperature is the only dependent variable and the energy conservation equations are written separately for the solid and the liquid regions. The major difficulty with this technique arises from the need to track a continuously moving phase change interface. The rate of propagation of this boundary into the solid region (melting) or into the liquid region (solidification) depends on the temperature gradients on both sides of the boundary, which are unknown *a priori*. Various procedures have been developed to deal with this problem, including moving grid points and isotherm migration [3, 7–10]. In the second group, known as the enthalpy method, both the enthalpy and the temperature are used as dependent variables in the energy equation. The resulting equation is applicable at all the grid points in the solid and in the liquid regions as well as those containing the solid–liquid interface. Carslaw and Jaeger [2] and Shamsundar and Sparrow [11] demonstrated the equivalence between the enthalpy formulation and the conduction energy equation assuming equal densities for both phases. In the conventional enthalpy method the solid–liquid energy boundary condition is not utilized and the problem reduces to one of nonlinear heat conduction. The location of the phase change interface is determined from the calculated enthalpies.

The enthalpy method is reasonably accurate for metals which undergo a change of phase over a temperature range. However, for materials with a change of phase which takes place at a single temperature, the enthalpy method is inaccurate in the region near the phase front. Voller *et al.* [12, 13] used the enthalpy method for water, and showed that (i) the calculated phase change boundary moved in an oscillatory fashion and (ii) the temperature history contained a number of plateaus. These nonphysical features resulted for water because of the large value of the ratio of the latent heat to the change in enthalpy of the sensible heat. Voller and Cross [13] and Tacke [14] have proposed techniques to improve the accuracy of the enthalpy formulation. A review of the enthalpy formulation can be found in refs. [11, 15].

In a study of rapid melting and solidification during pulsed laser heating, Hsu *et al.* [16] employed an enthalpy formulation similar to that used by Shamsundar and Sparrow [11]. The temperature history of

† Present address: Department of Mechanical Engineering, Isfahan University of Technology, Isfahan, Iran.

NOMENCLATURE

a	thermal diffusivity [$m^2 s^{-1}$]
b	defined by equation (A1)
c	specific heat [$J kg^{-1} K^{-1}$]
e	specific enthalpy [$J kg^{-1}$]
g	rate of heat generation [$W m^{-3}$]
h	defines the beam temporal shape [dimensionless]
I_0	beam intensity at the center [$W m^{-2}$]
I_a	beam intensity inside the target [$W m^{-2}$]
I_s	beam intensity incident on the surface [$W m^{-2}$]
k	thermal conductivity [$W m^{-1} K^{-1}$]
L	latent heat of fusion [$J kg^{-1}$]
q_a	absorbed energy flux, $I_s(1-R)$ [$W m^{-2}$]
r; R	radial distance [m]; reflectivity
S	solid–liquid interface location [m]
t; t_p	time; pulse duration [s]
T	temperature [K]
w	beam radius [m]
x	mass fraction of the liquid phase [dimensionless]
z	axial distance [m].

Greek symbols

α	absorption coefficient [m^{-1}]
δ_t	thermal diffusion length, $2\sqrt{(\alpha_s t_p)}$ [m]
ε	surface emissivity
ρ	density [$kg m^{-3}$]
σ	Stefan–Boltzmann constant [$W m^{-2} K^{-4}$].

Subscripts

av	average
b	boiling
e	east side (Fig. 17)
i	initial
j	refers to region 1, 2, or 3
l	liquid
m	melting
ml	defined in Fig. 2
ms	defined in Fig. 2
n	north side (Fig. 17)
p	center (Fig. 17)
pp	defined in the Appendix
s	solid; south side (Fig. 17)
w	west side (Fig. 17)
1	region 1
2	region 2.

the target was not presented in the paper of Hsu *et al.* [16] and therefore it is not possible to determine whether temperature plateaus were obtained as were reported by Voller *et al.* [12, 13]. However, since it is assumed that the grid point temperature remains at the melting point during the period of time that the melt front is traveling through the corresponding mesh, temperature plateaus presumably did exist. The period of time during which the temperature of each grid point remains constant depends on the size of the mesh. For a mesh size in the direction of the laser beam that is one tenth of the average thickness of the melt layer created by one pulse, it would take approximately 10% of the pulse duration for the interface to pass across each mesh. During this time the temperature of the corresponding mesh would remain constant. Since the heat affected region may be much larger than the depth of the melt, reducing the size of the mesh would result in very large computer time and storage requirements. Therefore, a modification to the traditional enthalpy method seems appropriate.

In this study an explicit finite difference scheme incorporating the enthalpy formulation was employed to calculate the temperature distribution and the location of the solid–liquid interface in a material undergoing melting and solidification. The time range considered in this work was from 1 ns to 100 ms. The enthalpy method was modified by making use of the following: (i) only a portion of the net energy transferred to a mesh is used for the phase change and the rest is used for the sensible energy change, and (ii) the thermal resistances between a grid point and the neighboring points separated by the interface involve two phases with different thermal conductivities. Note that the thermal conductivities of liquid metals are almost half of the values for the solid phase. For aluminum, the thermal conductivities of the solid and liquid at the melting point are 208 and 108 W m^{-1} K^{-1} respectively.

The problem studied in this work is that of two-dimensional (axisymmetric) melting and solidification of a substance resulting from the application of a pulsed beam on its surface. The radiation absorbed is included as a heat source whose strength varies with time and position. The variation with temperature of the thermophysical and the optical properties of the target material are included in the calculations. It is assumed that the surface temperature does not reach the boiling temperature of the target material. The model is applicable to substances that have a discrete phase change temperature and also to those that undergo a change in phase over a temperature range.

PROBLEM STATEMENT

A slab of the target material (see Fig. 1) is irradiated over a circular region of its surface by a laser beam of prescribed spatial and temporal distribution. The radial and axial dimensions of the target are much greater than the thermal diffusion length so that a

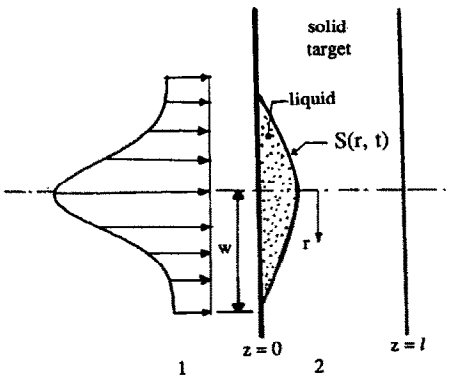

FIG. 1. Physical model for the problem showing beam irradiation.

thermally semi-infinite region is assumed. The intensity of the beam is a maximum at the optical axis, $r = 0$, and decreases radially and axially in the material. For thermal analyses, a commonly used radial distribution for lasers is the cylindrically symmetric Gaussian profile [17]:

$$I_s(r, t) = I_0 h(t) e^{-(r^2/w^2)} \tag{1}$$

where $h(t) \leqslant 1$ describes the temporal variation of the beam, which is a dimensionless quantity. If the intensity of the incident beam does not vary with time, $h(t) = 1$. The local radiation intensity within the target material, I_a, considering volumetric absorption and surface reflection, may be written as

$$I_a = I_s(1-R)e^{-\alpha z}. \tag{2}$$

It is pointed out that reflections at the solid–liquid interface may be neglected because the absorption is strong so that little radiation reaches the interface. The energy absorbed may be represented as a heat source within the material having a rate of heat generation per unit volume, g, given by [18]:

$$g = -\frac{dI_a}{dz} = \alpha I_s(1-R)e^{-\alpha z}. \tag{3}$$

The diffusion equation may be written in terms of enthalpy [11]. For two-dimensional transport with heat generation the equation is given by

$$\frac{1}{r}\frac{\partial}{\partial r}\left(k_j r \frac{\partial T_j}{\partial r}\right) + \frac{\partial}{\partial z}\left(k_j \frac{\partial T_j}{\partial z}\right) + g_j = \rho_j \frac{\partial e_j}{\partial t} \tag{4}$$

where e is the enthalpy and $j = 1, 2$ corresponds to the regions shown in Fig. 1. For region 1, which is usually air, $g_1 = 0$ and $\rho_1(\partial e_1/\partial t)$ is replaced by $\rho_1 c_1(\partial T_1/\partial t)$. Equation (4) is used for each discretized spatial domain, which by appropriate substitution of thermophysical properties will be valid regardless of whether the domain is in the solid state, the liquid state, or contains the solid–liquid interface. The interface in this case is axisymmetric. At the interface the following conditions hold [19]:

$$T_s = T_l = T_m \tag{5}$$

$$\left[1 + \left(\frac{\partial S}{\partial r}\right)^2\right]\left[k_s \frac{\partial T_s}{\partial z} - k_l \frac{\partial T_l}{\partial z}\right] = \rho L \frac{\partial S}{\partial t} \tag{6}$$

where L is the latent heat of fusion of the target material. Equation (6) represents the energy balance across the phase boundary; i.e. $z = S(r, t)$. Note that the complete energy balance across the phase boundary would require two equations corresponding to the axial and radial directions [19]. In this study the interface is divided into a series of steps for each grid point which are taken to be perpendicular to the z-direction. Therefore the equation in the radial direction is not utilized.

The relationship between the enthalpy and temperature is now considered. For a binary phase change this variation is assumed to be a piecewise linear function within the mushy zone with a step function change at the solid temperature, T_{ms} (see Fig. 2). The enthalpy–temperature relations for any element that is completely in the solid or in the liquid phase are given as follows:

$$e_s = \int_{T_{ms}}^{T} c_s \, dT \qquad T < T_{ms}, \tag{7a}$$

$$e_l = \int_{T_{ml}}^{T} c_l \, dT + L \qquad T > T_{ml}. \tag{7b}$$

The solid state at the melting temperature is chosen as the reference point with an enthalpy of zero. For a mesh containing the interface the average enthalpy is defined as

$$e = xe_l + (1-x)e_s \tag{8}$$

where x is the mass fraction of the mesh in the liquid phase. By using an average value for the specific heat and employing equations (7a) and (7b), equation (8) is expressed as

$$e = xL + c_{av}[(T - T_{ms}) + x(T_{ms} - T_{ml})]. \tag{9}$$

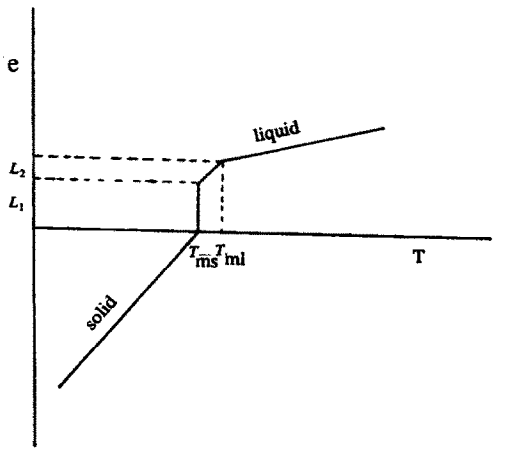

FIG. 2. Enthalpy–temperature relation.

In the present work the materials studied have a change of phase at a single temperature. Equations (7a), (7b) and (9) may be used for this condition by using $T_{ms} = T_{ml} = T_m$. Note that by writing equation (9) for a mesh (instead of a grid point) it is possible to obtain the phase change boundary at every time step, as discussed later.

The initial condition for equation (4) is a uniform temperature, $T = T_i$, everywhere. The boundary conditions at the surface $z = 0$ are

$$T_1 = T_2 \tag{10a}$$

$$k_1 \frac{\partial T_1}{\partial z} = k_2 \frac{\partial T_2}{\partial z} - \varepsilon\sigma(T_2^4 - T_i^4). \tag{10b}$$

At the extreme boundaries the conditions are

$$z \to \infty, \quad T_2 = T_i \tag{11a}$$

$$z \to -\infty, \quad T_1 = T_i. \tag{11b}$$

From symmetry we have

$$r = 0, \quad \frac{\partial T_1}{\partial r} = 0, \quad \frac{\partial T_2}{\partial r} = 0. \tag{12}$$

Far from the axis of the beam, for any value of z, we have

$$r \to \infty, \quad T_1 = T_2 = T_i. \tag{13}$$

The location of the solid–liquid interface is obtained from equation (6). The enthalpy and the temperature are calculated from equations (4), (7) and (9).

NUMERICAL METHOD

The first step in the computational process is to subdivide regions 1 and 2 into a number of small elements. Figure 3 shows the pattern of the grid points used in our calculations. The grid points are fixed in space while the interface moves in the target. The grid sizes used in the calculations were approximately determined from $\Delta z_1 \approx \delta_{t1}/m_1$, $\Delta z_2 \approx \delta_{t2}/m_2$ and $\Delta r = a/n$; δ_{t1} and δ_{t2} being the thermal diffusion lengths in air and the target material at room temperature. Values of $m_1 = m_2 = 50$ and $n = 10$ were used throughout the calculations. However, because of the large range of the time periods from milliseconds to microseconds, the grid sizes in the z-direction were different for different cases. For example, for a millisecond pulse $\Delta z_1 = \Delta z_2 = 12$ μm, for a microsecond pulse $\Delta z_1 = \Delta z_2 = 0.4$ μm, and for a nanosecond pulse $\Delta z_1 = \Delta z_2 = 0.012$ μm were used. A radial spacing of $\Delta r = 10$ μm was used for all cases. The temperature distribution and the melt pool size did not change noticeably when the mesh was refined with a factor of 1.5 for the millisecond case.

The finite difference form of equation (4) for the internal grid points of region 2 in the explicit formulation is given by

$$e_2'(i,j) = \frac{[a_s T_2(i-1,j) + a_n T_2(i+1,j) + a_e T_2(i,j+1) + a_w T_2(i,j-1) + a_p T_2(i,j) + a_{pp} e_2(i,j) + b]}{a_{pp}}. \tag{14}$$

All the quantities on the right hand side of equation (14) correspond to the previous time step, while $e_2'(i,j)$ corresponds to the new time. The coefficients a_s, a_n, a_w and a_e include the thermal resistances between the grid points. Composite resistances are accounted for due to the presence of two phases between the grid points adjacent to the solid–liquid interface. The coefficients a_{pp} and a_p include the mass and the specific heat of the element, respectively, and b represents the heat generation within the element. These coefficients are given in the Appendix. They are calculated at every time step to account for the changes in the thermophysical properties with temperature and

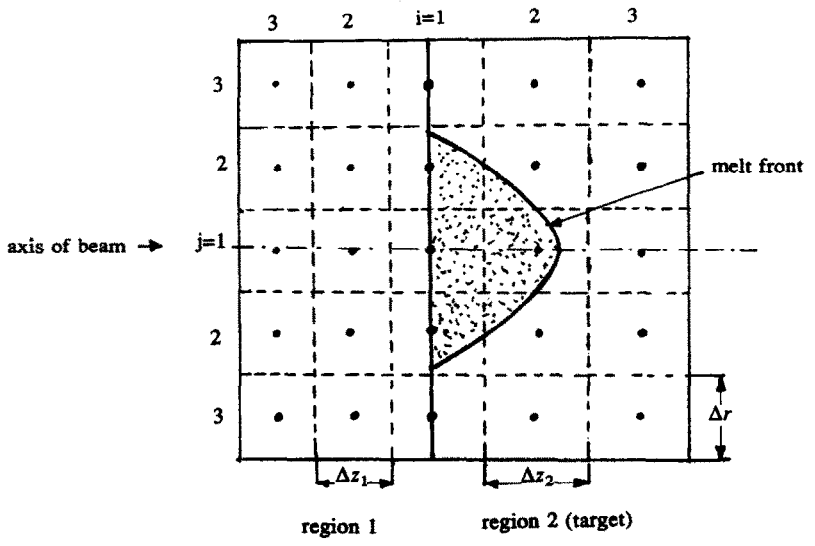

FIG. 3. Grid pattern used in the numerical solution.

change of phase. The corresponding finite difference equation for the surface element of the target, $z = 0$, is

$$e'_2(i,j) = \frac{[a_s T_1(i+1,j) + a_n T_2(i+1,j) + a_e T_2(i,j+1) + a_w T_2(i,j-1) + a_p T_2(i,j) + a_{pp} e_2(i,j) + b]}{a_{pp}}. \quad (15)$$

Here, b includes the radiation heat loss to the surroundings in addition to the heat generation inside the element. The grid points at the surface of the target represent elements containing materials of both regions 1 and 2. In order to eliminate the ambiguity concerning the definition of a single enthalpy for a composite element, the mass of air in these elements is neglected compared to the mass of the target material. This assumption does not have a significant effect on the accuracy of the results as long as the density of material 1 (air in this example) is much smaller than that of the target. For the internal grid points of region 1, the conduction equation is written in a finite difference form [18].

We apply the finite difference form of equation (6) to the solid–liquid interface. Figure 4 shows the volume element (i, j) containing the interface and its neighboring elements at time t. The interfacial surface S at this time divides the average length of an internal element into a liquid portion $x\Delta z$ and a solid portion $(1-x)\Delta z$. After a small increment in time, Δt, the interface moves to a new location S', resulting in an increase (melting) or decrease (solidification) of the liquid portion. The new location of the interface can be found from the finite difference form of equation (6):

$$\left[1+\left(\frac{S(i,j+1)-S(i,j)}{\Delta r}\right)^2\right]\left[k_s \frac{T_2(i+1,j)-T_m}{(1-x)\Delta z+\frac{\Delta z}{2}} - k_l \frac{T_m - T_2(i-1,j)}{\frac{\Delta z}{2}+x\Delta z}\right] = \rho L\left(\frac{S'(i,j)-S(i,j)}{\Delta t}\right). \quad (16a)$$

Recall that the subscript in T_2 simply refers to the target material. Note that the new location of the interface is determined by assuming that the change in the interface at any r position occurs only in the z-direction. However, it is emphasized that the change in the interface does vary with the radial position. If the interface is in a surface element of the target, the corresponding equation would be

$$\left[1+\left(\frac{S(i,j+1)-S(i,j)}{\Delta r}\right)^2\right]\left[k_s \frac{T_2(i+1,j)-T_m}{(2-x)\frac{\Delta z}{2}} - k_l \frac{T_m - T_2(i,j)}{x\frac{\Delta z}{2}}\right] = \rho L\left(\frac{S'(i,j)-S(i,j)}{\Delta t}\right). \quad (16b)$$

Once $S'(i, j)$ is calculated it can be used to obtain the liquid portion x' at time $t+\Delta t$.

At the onset of melting, $x = 0$, equation (16b) becomes infinite. This singularity is removed by writing equation (16b) in an implicit form. Therefore, for the starting condition we have

$$\left[k_s \frac{T'_2(i+1,j)-T_m}{(2-x')\frac{\Delta z}{2}} - k_l \frac{T_m - T'_2(i,j)}{x'\frac{\Delta z}{2}}\right] = \rho L \frac{S'(i,j)}{\Delta t}. \quad (17)$$

Unlike equations (16), which have only one unknown, $S'(i, j)$, equation (17) has three unknowns, namely $S'(i, j)$, x' and $T'_2(i, j)$. The last two parameters can be eliminated by using equation (9) and the relation $S'(i, j) = x'(\Delta z/2)$.

Determination of the temperature distribution and

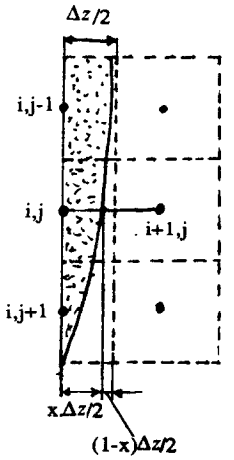

(a) internal meshes

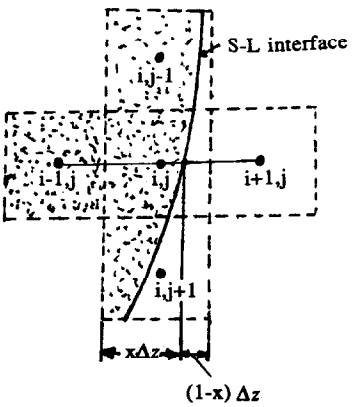

(b) surface meshes

FIG. 4. Grid points near the solid–liquid interface.

the solid–liquid interface involves the following procedure. The enthalpy of each grid point is calculated from equation (14) or (15). For the first time step, the temperature of each grid point is calculated from equation (7). Then the temperatures of the surface grid points are compared with the melting temperature, T_m. If all of these temperatures are less than the melting temperature there is no phase change and the calculations continue for the next time step following the above procedure. If any surface temperature is greater than the melting temperature, the solid–liquid interface is assumed to be in that mesh. The initial location of the solid–liquid interface is then calculated from equation (17). For the next time step, equation (16b) is then used to determine its location as long as the interface remains in a surface mesh. Once the interface moves into an internal mesh, equation (16a) is used. The grid point temperatures of the meshes that are completely in the solid or in the liquid phase are calculated from equations (7a) or (7b), respectively. The temperatures of the meshes containing the solid–liquid interface are calculated from equation (9).

The thermophysical properties used in the calculations were obtained from Touloukian and Ho [20] and Rohsenow and Hartnett [21]. For a commercially pure aluminum medium these properties are approximated as follows:

Thermal conductivity

$$k_s = 226.67 + 0.033T \quad 300\,\text{K} < T \leqslant 400\,\text{K} \tag{18a}$$

$$k_s = 264 - 0.055T \quad 400\,\text{K} < T \leqslant 933\,\text{K} \tag{18b}$$

$$k_l = 63 + 0.03T \quad 933\,\text{K} < T \leqslant 1600\,\text{K} \tag{18c}$$

$$k_l = 114 \quad 1600\,\text{K} < T \leqslant 2723\,\text{K} \tag{18d}$$

Specific heat

$$c_{ps} = 0.762 + 4.67 \times 10^{-4} T \quad 300\,\text{K} < T \leqslant 933\,\text{K} \tag{19a}$$

$$c_{pl} = 0.921\,\text{kJ kg}^{-1}\,\text{K}^{-1} \quad T > 933\,\text{K} \tag{19b}$$

Density

$$\rho_s = 2767 - 0.22T \quad 300\,\text{K} < T < 933\,\text{K} \tag{20a}$$

$$\rho_l = 2640 - 0.275T \quad 933\,\text{K} < T < 1400\,\text{K}. \tag{20b}$$

The time steps used in the calculations varied for different cases. Values from $\Delta t = 3 \times 10^{-13}$ s (for the nanosecond case) to 3×10^{-8} s (for the millisecond case) were used. Calculations were also made with a time step of $\Delta t = 1.5 \times 10^{-8}$ s for the millisecond case. The results were virtually identical.

RESULTS AND DISCUSSION

The results of the present model were compared with the experimental data of Clough *et al.* [22], who presented results for the final melt depth profile in a 1100 aluminum alloy target. A rectangular plate sample with dimensions of $40 \times 15 \times 4$ mm^3 was heated with a 100 ms duration stationary electron beam having a uniform intensity over a circular cross-section with a 1 mm radius. The beam energy is completely absorbed by the target. Therefore, the calculations were made with $R = 0$. A value of $\alpha = 1 \times 10^9$ m^{-1} has been used [17]. Photographs of the final melt depth profiles were obtained for several energy fluxes using an acoustic emission method [22].

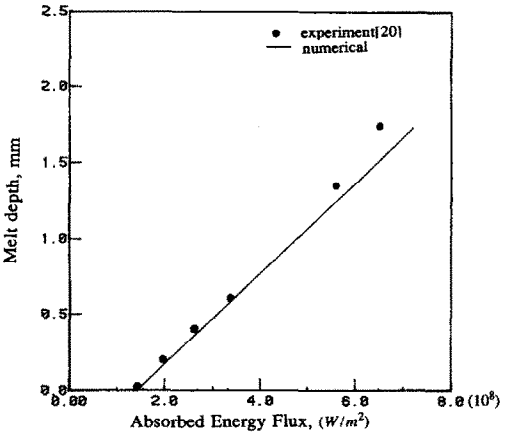

FIG. 5. Maximum melt depth vs absorbed energy flux for a 100 ms pulse.

Figure 5 shows the maximum depth of the melt at the end of a 100 ms pulse for different absorbed energy fluxes, $q_a = I_s$, for $R = 0$. The agreement between the experimental data and the numerical results is very good for fluxes less than $q_a = 6 \times 10^8$ W m^{-2}. However, at the higher energy fluxes the model underpredicts the data. This disagreement is due to the fact that the model assumes that the surface temperature does not reach the boiling point (2723 K). This assumption is not valid for high energy fluxes because the surface reaches the boiling point during the early stages of pulse heating. Figure 6 shows the time that is calculated for the surface temperature of the aluminum target at $r = 0$ to reach the boiling point with

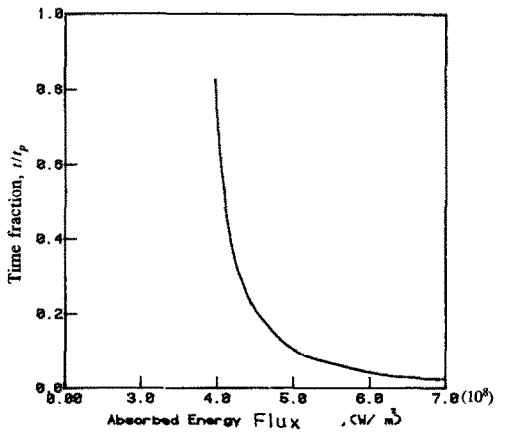

FIG. 6. Time needed for the surface temperature at $r = 0$ to reach boiling point.

a CW uniform intensity laser beam. Note that for $q_a = 6 \times 10^8$ W m^{-2} it takes only 6% of the pulse duration for the surface temperature at $r = 0$ to reach the boiling point (more time is needed at larger distances from the beam axis). From Fig. 5 it is seen that for this high energy flux the calculated melt depth is still in fair agreement with the experimental data. This can be explained as follows. Once the surface temperature reaches the boiling point, a portion of the energy is used to vaporize the material and less energy is available for melting. If the energy deposition does not cause melt ejection, the process will be one of simple vaporization, with the surface remaining at the boiling point and recessing due to the material removal (due to evaporation). Consequently, there are two opposing factors acting on the progress of the melt depth. The penetration of the high temperature surface toward the interface resulting from evaporation tends to increase the actual melt depth (a factor that is ignored in the model), while the smaller amount of energy available for melting tends to decrease the melt depth (also ignored in the model). These opposing effects apparently yield the fair agreement between the numerical model and the experimental data at the higher energy fluxes.

Figure 7 shows the final solid–liquid interface profiles for the aluminum target that was irradiated with 100 ms pulses for two different energy fluxes. The predictions lie somewhat below the experimental data in the central region and above the data in the outer region. This difference may be due to the fact that the target is not thermally semi-infinite; that is, the thickness, 4 mm, is comparable to the thermal diffusion length. Figure 8 shows the calculated surface temperature of the same target at $r = 0$ as a function of time for different values of the absorbed energy flux. Note that the time calculated for melting to begin (at 933 K) is almost the same over the range of the absorbed fluxes studied. Although the surface reaches the boiling point (2723 K) very quickly for the highest flux, it does not reach that value for the two smaller

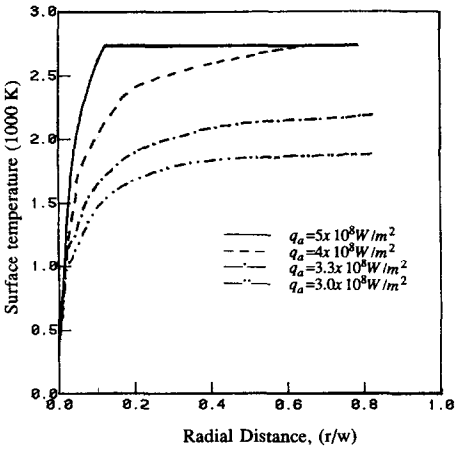

FIG. 8. Surface temperature at $r = 0$, $t_p = 100$ ms for different absorbed energy levels.

fluxes. For $q_a < 4 \times 10^8$ W m^{-2}, the temperature increases continuously with time, and a change in the slope of the temperature profile results due to melting.

Calculations were made over a range of pulses varying from nanosecond to millisecond durations. The effects of laser pulse duration on the aluminum surface temperature and the melt depth are shown in Figs. 9–14. The results during the cooling period are also included in these figures. For these calculations a uniform intensity beam was used in which the intensity was changed stepwise at $t = 0$ and remained constant during the pulse duration (rectangular temporal shape). The beam diameter was 200 μm; other beam parameters are given in Table 1.

As the pulse duration was increased from case 1 to 6, the absorbed energy flux was decreased in order to keep the surface temperature below the boiling point. The values of the heat fluxes in the table were varied according to $1/\sqrt{t_p}$, except for the smallest energy input; namely case 6.

Figure 9 shows the surface temperatures of the aluminum target at $r = 0$. For the millisecond pulse,

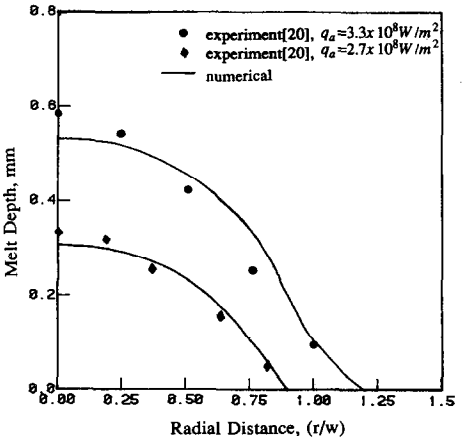

FIG. 7. Steady state melt depth for a 100 ms pulse.

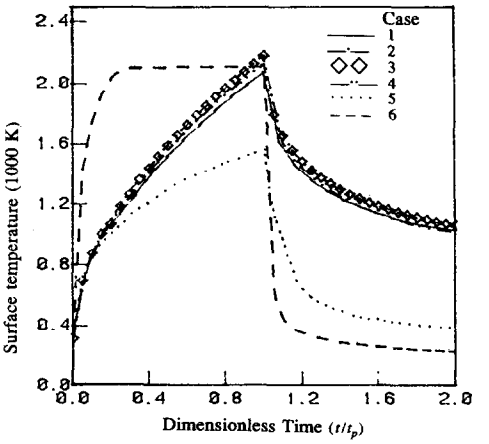

FIG. 9. Surface temperature vs time for different pulses.

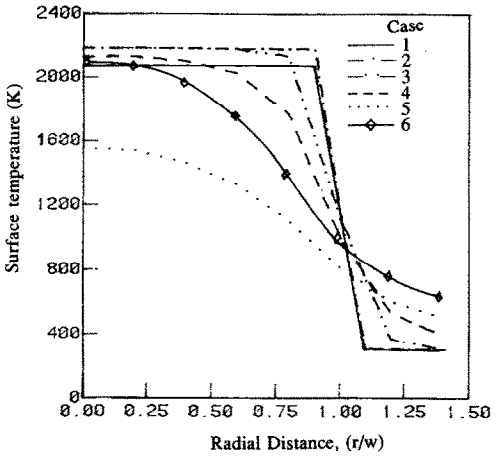

FIG. 10. Surface temperature profiles at the end of the pulse.

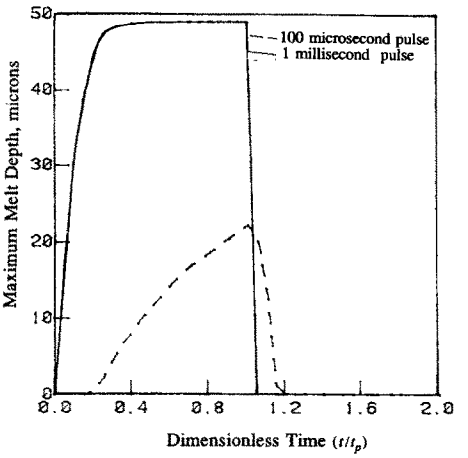

FIG. 13. Maximum melt depth vs time for 100 μs and 1 ms pulses.

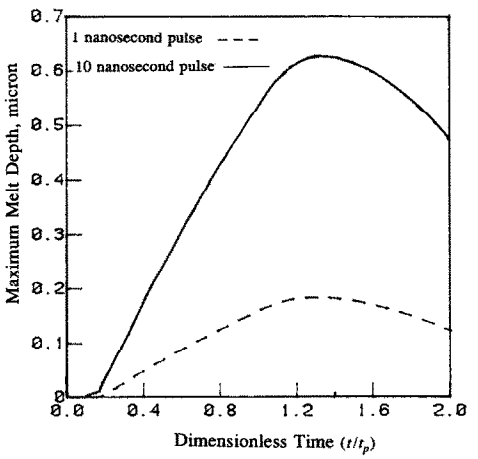

FIG. 11. Maximum melt depth vs time for 1 and 10 ns pulses.

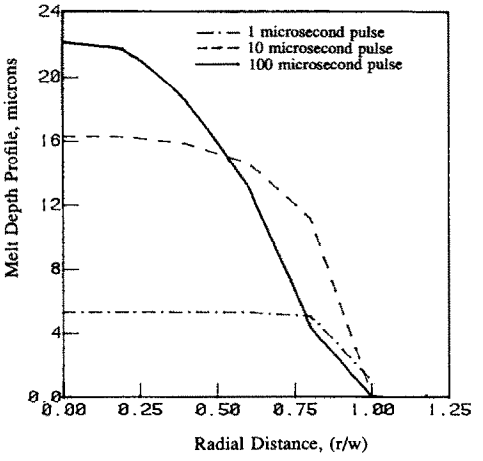

FIG. 14. Melt depth profiles at the end of the pulse.

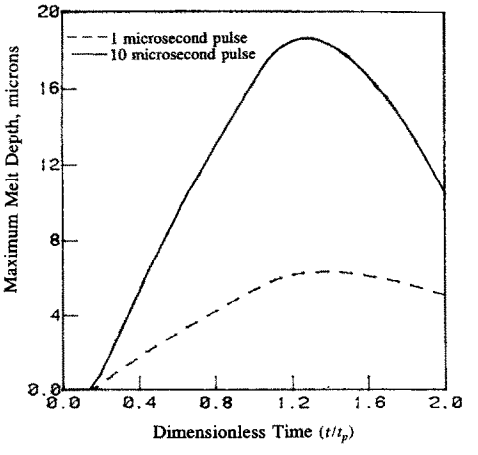

FIG. 12. Maximum melt depth vs time for 1 and 10 μs pulses.

case 6, the temperature quickly reaches a constant value (in terms of dimensionless time, t/t_p) and drops sharply after the end of the pulse. For shorter pulses (cases 1–5), the surface does not reach a constant value during the heating pulse. After the removal of the power at $t/t_p = 1$, the surface temperature decreases for all of the cases. However, at $t/t_p = 2$, the temperature does not return to the initial temperature except for case 6. At this time the heating pulse begins

Table 1. Energy fluxes and pulse durations

Case	Pulse duration (s), t_p	Energy flux (W m^{-2}), q_a
1	1E−9	9.5E+11
2	1E−8	3.18E+11
3	1E−6	3.18E+10
4	1E−5	9.68E+9
5	1E−4	3.18E+9
6	1E−3	3.5E+9

again (not shown) and the surface temperature is now at a higher value for cases 1–5. Figure 9 shows that for pulses shorter than or equal to 10 μs (cases 1–4) the variations of the surface temperature at $r = 0$ with respect to the nondimensionalized time are approximately the same. Since the absorbed energy flux was varied inversely proportional to $\sqrt{t_p}$, it is concluded that the maximum surface temperature (that is, at $r = 0$) for short pulses can be predicted from

$$(T - T_i)_{max} = C_1 q_a \sqrt{t_p} \tag{21}$$

where C_1 is a function of the thermophysical properties of the target material (T, K; q_a, W m^{-2}; t_p, s). From the results shown in Fig. 9, a value of $C_1 = 5.91 \times 10^{-5}$ K m^{-2} W$^{-1/2}$ was obtained. The temporal variation of the temperature at $r = 0$ during these heating pulses can be estimated from:

$$T(r = 0, t) - T_i = C_1 q_a \sqrt{t}. \tag{22}$$

Equation (22) is of the form given by the analytical solution for a one-dimensional semi-infinite solid that is heated uniformly at the surface without a change of phase. This conclusion is of a general nature and should be valid for values other than those given in Table 1 provided that the pulse duration is short and no vaporization takes place. Equation (22) is useful for predicting the range of the energy fluxes that are needed for surface melting without permanent damage (vaporization). These values are given in Table 2 for different uniform intensity pulses. The values of q_{am} and q_{ab} are calculated from equation (22) by using $T = T_m$ and $T = T_b$, respectively. q_{ab} is the amount of absorbed heat flux needed to increase the surface temperature of the target at the center of the beam to the boiling point of aluminum at the end of the pulse. In general, the threshold intensity depends on the pulse duration and the temporal and the spatial distribution of the incident beam. McKay *et al.* [23] reported a threshold absorbed peak flux of 1.25×10^{10} W m^{-2} for an aluminum target irradiated by a CO_2 laser ($\lambda = 10.6$ μm) with a pulse duration of 1.8 μs. Equation (22) gives $q_{ab} = 2.74 \times 10^{10}$ W m^{-2}. Much lower threshold absorbed heat fluxes, of the order of 10^8 W m^{-2} were also reported [24].

Figure 10 shows the surface temperature profile at time $t/t_p = 1$ for the various pulse durations, t_p. The results show that the shorter the pulse the more uniform is the temperature. For pulses shorter than or equal to 1 μs the problem can be considered to be one-dimensional because of the small thermal diffusion length in comparison to the beam diameter. Equations (21) and (22) are valid as long as the one-dimensional approximation is valid. This approximation fails for pulses longer than 10 μs; that is, cases 5 and 6 (note that for case 4, $t_p = 10$ μs, the approximation begins to be less accurate). The results for the melt depth at the center of the beam ($r = 0$) for different pulses are plotted versus dimensionless time in Figs. 11–13. As the duration of the pulse is increased the maximum melt depth increases. For pulses shorter than 10 μs the maximum depth occurs after the end of the pulse. The time lag increases as the pulse duration decreases. Figures 11 and 12 show that the solidification front does not reach the surface during the short cooling periods for these cases. The maximum melt depth for the millisecond pulse (cf. Fig. 13) is two orders of magnitude greater than that for the nanosecond pulse (cf. Fig. 11). The velocity of the solid–liquid boundary, which represents the rate of melting or solidification, is of the order of 200 m s^{-1} for the nanosecond pulse and 0.5 m s^{-1} for the millisecond pulse.

Figure 14 shows the radial distribution of the melt depth at the end ($t/t_p = 1$) of three different pulses. Again, the radial dependence may be neglected for pulses shorter than or equal to 1 μs.

Figures 15 and 16 show the results for a more practical pulse. Here the spatial distribution of the intensity is given by a Gaussian profile, $I = I_0 e^{-(r^2/w^2)}$, and a triangular temporal variation is used (with the intensity increasing linearly from zero at the beginning of the pulse to a maximum value at $t/t_p = 0.5$, then decreasing linearly to zero at $t/t_p = 1$ and then remaining at zero). The maximum flux at the center of the beam, I_0, is 1.91×10^{12} W m^{-2} with a beam diameter of 200 μm. Figure 15 shows the solid–liquid interface at different times. In contrast to the case of a uniform intensity nanosecond pulse (cf. Fig. 10, case 1) the melt depth changes considerably in the radial direc-

Table 2. Ranges of absorbed energy for melting of aluminum

Pulse duration (s)	q_{am} (W m^{-2})	q_{ab} (W m^{-2})
1E−5	3.39E+9	1.3E+10
1E−6	1.07E+10	4.09E+10
1E−7	3.39E+10	1.29E+11
1E−8	1.07E+11	4.09E+11
1E−9	3.39E+11	1.29E+12

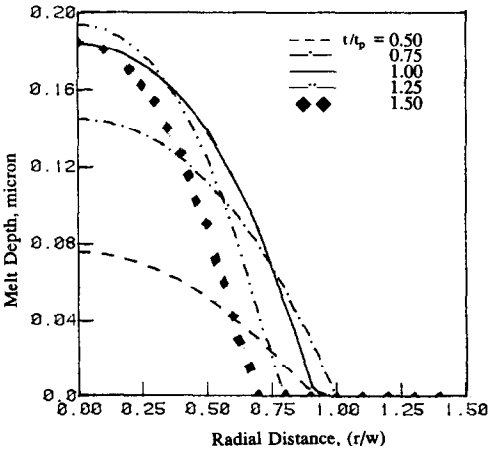

FIG. 15. Solid–liquid boundary profiles for nonuniform triangular temporal shape nanosecond pulse.

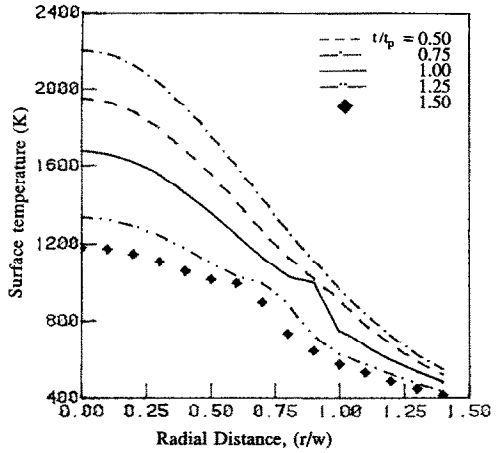

FIG. 16. Surface temperature profiles for nonuniform triangular temporal shape nanosecond pulse.

tion and the one-dimensional approximation is no longer valid. Note that the maximum depth of the melt zone increases with time until $t/t_p = 1.25$, and then begins to decrease; the radius begins to decrease after $t/t_p = 0.75$. Therefore, the time $t/t_p = 1$ cannot be simply used as the only characteristic time that is needed to describe all the complex variations that are taking place. The actual temporal variations of the heat flux and the properties of the material must also be considered. The longer diffusion time from the surface to the depth of the melt zone results in a slower response to the temporal variation of the incident radiation. The result is a radial shrinking of the melt region. Figure 16 shows the surface temperature profiles at different times. After $t/t_p = 0.75$, the temperatures over the entire surface decrease with time and a decrease in the radial gradient is observed. Note that the radial temperature gradient is two orders of magnitude smaller than the axial (z-direction) gradient. We again note that the actual magnitudes of the unsteady heat fluxes are important and it is difficult to generalize the results.

CONCLUSIONS

The enthalpy method was modified and applied to the problem of rapid melting and solidification of a substance resulting from the application of a pulsed laser beam. The temperature plateau which usually results when the enthalpy method is used was eliminated by using energy boundary condition at the solid–liquid interface. Good agreement was obtained between the predictions and experimental data for the melt depth profile in an aluminum target. The results of calculations for a range of pulse durations from nanoseconds to milliseconds have shown that for short pulses the radial dependence of the melt depth and the temperature become similar to the radial distribution of the intensity of the laser beam. For short pulses with a spatially and temporally uniform intensity, a simple relation exists between the melt depth, the flux and the time. This relation can be used to predict the range of energy fluxes which can cause melting without material removal at the surface.

Acknowledgements—This work was supported by the Director, Office of Energy Research, Office of Basic Energy Sciences, Chemical Sciences Division, of the U.S. Department of Energy, under contract number DE-AC03-76SF00098. Support from the computing center of the University of California at Berkeley is gratefully acknowledged.

REFERENCES

1. L. Rubenstein, The Stefan problem, *Trans. Math. Monogr.* **22,** (1971).
2. H. S. Carslaw and J. C. Jaeger, *Conduction of Heat in Solids*, 2nd Edn. Oxford University Press, Oxford (1959).
3. J. R. Ockendon and W. R. Hodgkins (Editors), *Moving Boundary Problems in Heat Flow and Diffusion*. Oxford University Press, Oxford (1975).
4. V. Lunardini, *Heat Transfer in Cold Climates*. Van Nostrand Reinhold, New York (1981).
5. N. Shamsundar, Ph.D. Thesis, Department of Mechanical Engineering, University of Minnesota (1975).
6. M. Salcudean and Z. Abdullah, On numerical modeling of heat transfer during solidification processes, *Int. J. Numer. Meth. Engng* **25,** 445–473 (1988).
7. W. D. Murray and F. Landis, Numerical and machine solutions of transient heat conduction problem involving melting or freezing, *J. Heat Transfer* **81,** 106–112 (1959).
8. L. E. Goodrich, Efficient numerical technique for one dimensional thermal problems with phase change, *Int. J. Heat Mass Transfer* **21,** 615–621 (1978).
9. R. W. Lewis, K. Morgan and W. G. Habashi (Editors), *Numerical Methods in Thermal Problems—5, Proc. Fifth Int. Conf.*, Montreal, Canada, 29 June–3 July 1987. Pineridge Press, Swansea (1987).
10. A. Lazaridis, A numerical solution of the multidimensional solidification or melting problems, *Int. J. Heat Mass Transfer* **13,** 1459–1477 (1970).
11. N. Shamsundar and E. M. Sparrow, Analysis of multidimensional conduction phase change via the enthalpy model, *J. Heat Transfer* **97,** 333–340 (1975).
12. V. R. Voller, M. Cross and P. Walton, Assessment of weak solution techniques for solving Stefan problem. In *Numerical Methods in Thermal Problems* (Edited by R. W. Lewis and K. Morgan), p. 172. Pineridge Press, Swansea (1979).
13. V. R. Voller and M. Cross, Accurate solutions of moving boundary problems using the enthalpy method, *Int. J. Heat Mass Transfer* **24,** 545–556 (1981).
14. K. H. Tacke, Discretization of the explicit enthalpy method for planar phase change, *Int. J. Numer. Meth. Engng* **21,** 543–554 (1985).
15. V. Voller, Interpretation of the enthalpy in a discretized multidimensional region undergoing a phase change, *Int. Commun. Heat Mass Transfer* **10,** 323–328 (1983).
16. S. C. Hsu, S. Kou and R. Mehrabian, Rapid melting and solidification of a surface layer due to a stationary heat flux, *Metall. Trans.* **11B,** 29–38 (1980).
17. M. von Allmen, *Laser Interactions with Materials*. Springer-Verlag, New York (1987).
18. A. A. Rostami, R. Greif and R. E. Russo, Unsteady two dimensional heat transfer in laser heated materials. In *Transport Phenomena in Material Processing 1990*. ASME Publication HTD, Vol. 146 (1990).
19. M. N. Ozisik, *Heat Conduction*, pp. 397–438. John Wiley, New York (1980).
20. Y. S. Touloukian and C. Y. Ho (Editors), *Thermo-*

physical Properties of Matter, Vols 1 and 4. Plenum Press, New York (1972).
21. W. M. Rohsenow and J. P. Hartnett (Editors), *Handbook of Heat Transfer Fundamentals*, Chap. 3. McGraw-Hill, New York (1985).
22. R. B. Clough, H. N. G. Wadley and R. Mehrabian, Heat flow acoustic emission microstructure correlations in rapid surface solidifications. In *Lasers in Material Processing* (Edited by E. A. Metzbower), pp. 37–46. ASM, New York (1983).
23. J. A. McKay, R. D. Bleach, D. J. Nagel and J. T. Schriempf, Pulsed-CO_2-laser interaction with aluminum in air: thermal response and plasma characteristics, *J. Appl. Phys.* **50**, 3231–3240 (1979).
24. S. Marcus, J. E. Lowder and D. L. Mooney, Large-spot thermal coupling of CO_2 laser radiation to metallic surfaces, *J. Appl. Phys.* **47**, 2966–2968 (1976).

APPENDIX

Expressions will be given here for the coefficients in equations (14) and (15). Consider a grid point p surrounded by four grid points e, w, s, and n as shown in Fig. A1. For the internal grid points except for those located at $r = 0$, the following expressions are used:

$$a_e = k_{ep}\frac{\left(1+\frac{\Delta r}{2r_p}\right)\Delta z}{\Delta r^2}, \quad a_w = k_{wp}\frac{\left(1-\frac{\Delta r}{2r_p}\right)\Delta z}{\Delta r^2},$$

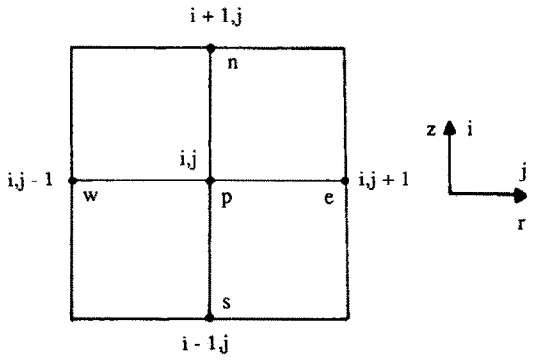

FIG. A1. Grid points for the numerical method.

$$a_n = \frac{k_{np}}{\Delta z}, \quad a_s = \frac{k_{sp}}{\Delta z}, \quad b = q_a$$

$$q_a = I_s(1-R)(e^{-\alpha z_i} - e^{-\alpha z_0}),$$

$$z_i = (i-1.5)\Delta z, \quad z_0 = (i-0.5)\Delta z$$

$$a_{pp} = \frac{\rho \Delta z}{\Delta t}, \quad a_p = -(a_e + a_w + a_n + a_s) \qquad \text{(A1)}$$

where k_{ep} is the average thermal conductivity between point e and p, etc. It can be expressed as:

$$k_{ep} = \frac{2k_e k_p}{k_e + k_p}. \qquad \text{(A2)}$$

For points located at $r = 0$, all the above relations are applicable except for a_e and a_w, which are given by

$$a_e = a_w = 4\frac{k_{ep}\Delta z}{\Delta r^2}.$$

Equation (A2) is good if both grid points e and p and the entire corresponding meshes are in a single phase. However, if the two neighboring grid points are separated by a solid–liquid interface, then the equivalent thermal conductivity between them can be obtained by referring to Fig. A2. For two points at the same z distance (see Fig. A2(a)), the expression is

$$k_{pq} = k_l x_q + k_s(1-x_p) + \frac{2k_s k_l}{k_s + k_l}(x_p - x_q) \qquad \text{(A3)}$$

where k_l and k_s are the thermal conductivities of the liquid and the solid phases at the melting point, respectively. For the two grid points at the same radial distance (see Fig. A2(b)) we get

$$k_{pq} = k_s k_l / (k_s x_{pq} + k_l(1-x_{pq})). \qquad \text{(A4)}$$

For the surface grid points ($z = 0$), the following expressions may be used except for the one at $r = 0$:

$$a_e = \frac{\left(1+\frac{\Delta r}{2r_p}\right)(k_{ep1}\Delta z_1 + k_{ep2}\Delta z_2)}{2\Delta r^2},$$

$$a_w = \frac{\left(1-\frac{\Delta r}{2r_p}\right)(k_{wp1}\Delta z_1 + k_{wp2}\Delta z_2)}{2\Delta r^2},$$

$$a_n = \frac{k_{np2}}{\Delta z_2}, \quad a_s = \frac{k_{sp1}}{\Delta z_1}, \quad b = q_a + b',$$

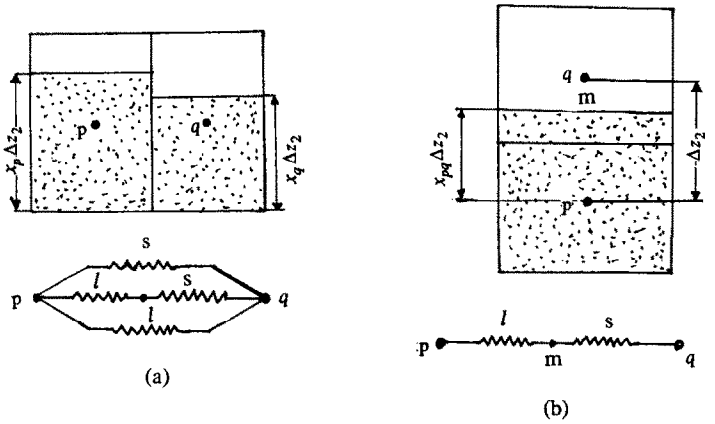

FIG. A2. Method of calculating thermal resistance between grid points.

$$q_a = I_s(1-R)(1-e^{-(\alpha\Delta z_2/2)}),$$
$$b' = \varepsilon\sigma(T_i^4 - T_p^4), \quad a_{pp} = \frac{\rho_2 c_2 \Delta z_2}{2\Delta t}. \qquad \text{(A5)}$$

For $r = 0$, the relations $a_e = a_w = 2(k_{ep1}\Delta z_1 + k_{ep2}\Delta z_2)/\Delta r^2$ are used. The other expressions given for the internal grid points are still applicable.

METHODE ENTHALPIQUE MODIFIEE APPLIQUEE AUX FUSIONS ET SOLIDIFICATIONS RAPIDES

Résumé—On étudie la solidification et la fusion rapides de matériaux types. La technique enthalpique est utilisée dans une forme explicite aux différences finies pour calculer la position de l'interface solide–liquide et la distribution de température dans le matériau. La technique a été modifiée de façon à ne pas nécessiter le maintien à la température de fusion pour l'interface. En utilisant la condition aux limites de l'énergie à l'interface, une nouvelle valeur de la température du point de la grille est calculée à chaque pas de temps. Les matériaux entre deux points de grille qui sont de chaque côté de l'interface sont deux phases qui ont des conductivités thermiques très différentes. Les résistances thermiques du matériau entre ces deux points sont calculées en traitant la région comme un matériau composite. Les effets de durée, la forme temporelle et l'intensité du laser pulsé sont étudies pour connaître la vitesse de propagation du changement de phase et la distribution de température. Les résultats de la prédiction numérique de la profondeur du bain créée dans un échantillon d'aluminium avec un faisceau d'électrons de 100 ms sont comparés avec des données expérimentales et on obtient un bon accord.

MODIFIZIERTES ENTHALPIE-VERFAHREN FÜR SCHNELLES SCHMELZEN UND ERSTARREN

Zusammenfassung—Es werden schnelle Schmelz- und Erstarrungsvorgänge untersucht. Der Verlauf der Fest-Flüssig-Phasengrenze sowie die Temperaturverteilung im Material wird mit einer expliziten Finite-Differenzen-Form des Enthalpie-Verfahrens berechnet. Das Verfahren wurde so modifiziert, daß die Temperatur des Gitterelements, in dem sich die Phasengrenze befindet, nicht konstant bei Schmelztemperatur bleiben muß. Stattdessen wird bei jedem Zeitschritt mit der Randbedingung für die Energie an der Phasengrenze ein neuer Temperaturwert für den Gitterpunkt berechnet. Zwischen den Gitterpunkten, welche die Phasengrenze einschließen, liegt das Material in zwei Phasen vor und weist daher sehr unterschiedliche Wärmeleitfähigkeiten auf. Zur Berechnung des Temperaturleitwiderstandes zwischen diesen Gitterpunkten wurde der Bereich als Verbundmaterial betrachtet. Die Einflüsse der Dauer, des zeitlichen Verlaufs und der Intensität des Laserpulses auf die Bewegung der Phasengrenze und der Temperaturverteilung wurden untersucht. Die Ergebnisse einer numerischen Vorausberechnung der Schmelztiefe in Aluminium bei Einwirkung eines Elektronenstrahls von 100 ms Dauer wurden mit experimentellen Daten verglichen. Es zeigte sich eine gute Übereinstimmung.

ПРИМЕНЕНИЕ МОДИФИЦИРОВАННОГО МЕТОДА ЭНТАЛЬПИИ К ПРОЦЕССУ БЫСТРОГО ПЛАВЛЕНИЯ И ЗАТВЕРДЕВАНИЯ

Аннотация—Исследовалось быстрое плавление и затвердевание материала мишени. Метод энтальпии в явной конечно-разностной форме использовался для определения положения границы раздела твердое тело – жидкость и распределения температур в мишени. Метод модифицировался таким образом, чтобы отсутствовала необходимость сохранения температуры ячейки, в которой находится граница раздела, постоянной и равной температуре плавления. С использованием условия для энергии на границе раздела рассчитывалось новое значение температуры в узлах сетки на каждом временном шаге. Материал между двумя узлами сетки, расположенными по обе стороны границы раздела, состоит из двух фаз с существенно различными коэффициентами теплопроводности. При определении теплового сопротивления соответствующая область рассматривалась как композитный материал. Исследовалось влияние длительности, формы и интенсивности лазерного импульса на скорость распространения фазового перехода и распределение температур. Результаты численного определения глубины расплава, образующегося в алюминиевой мишени под действием электронного импульса длительностью 100 мс, сравнивались с экспериментальными данными, и получено их хорошее согласие.